



HAL
open science

Superconductivity in the crystallogenide $\text{LaFeSiO}_{1-\delta}$ with squeezed FeSi layers

Mad F. Hansen, Jean-Baptiste Vaney, Christophe Lepoittevin, F. Bernardini,
Etienne Gaudin, V. Nassif, M.-A. Méasson, A. Sulpice, H. Mayaffre, M.-H.
Julien, et al.

► **To cite this version:**

Mad F. Hansen, Jean-Baptiste Vaney, Christophe Lepoittevin, F. Bernardini, Etienne Gaudin, et al.. Superconductivity in the crystallogenide $\text{LaFeSiO}_{1-\delta}$ with squeezed FeSi layers. *Npj Quantum Materials*, 2022, 7 (1), pp.86. 10.1038/s41535-022-00493-z . hal-03772788

HAL Id: hal-03772788

<https://hal.science/hal-03772788>

Submitted on 8 Sep 2022

HAL is a multi-disciplinary open access archive for the deposit and dissemination of scientific research documents, whether they are published or not. The documents may come from teaching and research institutions in France or abroad, or from public or private research centers.

L'archive ouverte pluridisciplinaire **HAL**, est destinée au dépôt et à la diffusion de documents scientifiques de niveau recherche, publiés ou non, émanant des établissements d'enseignement et de recherche français ou étrangers, des laboratoires publics ou privés.

Superconductivity in the crystallogenide LaFeSiO_{1-δ} with squeezed FeSi layers

M. F. Hansen,¹ J.-B. Vaney,² C. Lepoittevin,¹ F. Bernardini,³ E. Gaudin,² V. Nassif,^{1,4} M.-A. Méasson,¹ A. Sulpice,¹ H. Mayaffre,⁵ M.-H. Julien,⁵ S. Tencé,² A. Cano,¹ and P. Toulemonde^{1,*}

¹CNRS, Université Grenoble Alpes, Institut Néel, 38000, Grenoble, France

²CNRS, Université Bordeaux, ICMCB, UPR 9048, F-33600 Pessac, France

³Dipartimento di Fisica, Università di Cagliari, IT-09042 Monserrato, Italy

⁴Institut Laue -Langevin, 71 Avenue des Martyrs, 38000 Grenoble, cedex 9 France

⁵CNRS, LNCMI, Université Grenoble Alpes, INSA-T, UPS, EMFL, Grenoble, France

(Dated: May 2, 2022)

Pnictogens and chalcogens are both viable anions for promoting Fe-based superconductivity and intense research activity in the related families has established systematic correlation between the Fe-anion height and the superconducting critical temperature T_c , with an optimum Fe-anion height of ~ 1.38 Å. Here, we report the discovery of superconductivity in a novel compound LaFeSiO_{1-δ} that incorporates a crystallogen element, Si, and challenges the above picture: considering the strongly squeezed Fe-Si height of 0.94 Å, the superconducting transition at $T_c = 10$ K is unusually high. In the normal state, the resistivity displays non-Fermi-liquid behavior while NMR experiments evidence weak antiferromagnetic fluctuations. According to first-principles calculations, the Fermi surface of this material is dominated by hole pockets without nesting properties, which explains the strongly suppressed tendency towards magnetic order and suggests that the emergence of superconductivity materializes in a distinct set-up, as compared to the standard s_{\pm} - and d -wave electron-pocket-based situations. These properties and its simple-to-implement synthesis make LaFeSiO_{1-δ} a particularly promising platform to study the interplay between structure, electron correlations and superconductivity.

10 INTRODUCTION

11 Iron-based superconductors (IBSC) are presently a
12 well established class of unconventional superconductors,
13 spanning multiple structural families [1]. At their core,
14 IBSCs consist of a square planar lattice of Fe atoms,
15 tetrahedrally coordinated by pnictogen or chalcogen el-
16 ements X (typically $X = \text{As}$ or Se) placed above and
17 below the Fe plane. Different spacers can be intercalated
18 between this central structural unit, thereby forming the
19 different IBSC families. It turns out that the supercon-
20 ducting critical temperature (T_c) can be correlated with
21 the X anion height from the Fe plane $h_{\text{Fe-X}}$ (shown in
22 Fig. 2b), with the maximum $T_c \simeq 56$ K corresponding
23 to $h_{\text{Fe-X}} \sim 1.38$ Å [2, 3]. At the optimal height, the
24 FeX_4 tetrahedra becomes regular with the X -Fe- X angle
25 $\alpha = 109.47^\circ$. The IBSC class has recently been extended
26 to other layered materials where pnictogen/chalcogen
27 atoms are replaced by Ge in YFe_2Ge_2 and by Si in LaFe-
28 SiH and LaFeSiF _{x} [4–6]. This is very interesting because
29 it further establishes the prospect of finding more IBSCs.
30 Simultaneously, it is also surprising since the use of crys-
31 tallogens —*i.e.* group 14 elements— has been discussed
32 as detrimental to superconductivity since a ferromagnetic
33 ground state should become favoured as opposed to the
34 anti-ferromagnetic ground state which is normally asso-
35 ciated with the parent compounds of IBSCs [7].

36 In this work, we report a further extension of the iron-
37 crystallogen superconductors with the synthesis of the
38 novel compound LaFeSiO_{1-δ}. This compound represents

39 a new intriguing member of the so-called 1111 family
40 not only for evading ferromagnetism but also, and per-
41 haps more importantly, because of its exceptional crys-
42 tal structure (Fig. 2a) where the Fe-Si height drops to
43 0.94(1) Å. This parameter is far away from what is con-
44 sidered the optimal geometry for superconductivity in
45 the IBSCs, and indeed produces drastic changes in the
46 electronic properties as we show below. Yet, supercon-
47 ductivity is observed below onset $T_c = 10$ K with a small
48 $\delta = 10$ % oxygen deficit in the compound. This find-
49 ing thus challenges the current notion that crystallogens
50 should be avoided when searching for new IBSCs, and
51 provides a qualitatively new platform to further scruti-
52 nize the link between the crystal structure and the elec-
53 tronic properties in Fe-based superconductors.

54 RESULTS

55 Synthesis and Crystallographic structure

56 Polycrystalline LaFeSiO_{1-δ} samples were synthesized
57 from the non-superconducting, weak Pauli paramagnet
58 LaFeSi precursor [8] (see details in Methods). Fig. 1
59 shows the energy dispersive X-ray spectroscopy (EDX)
60 spectrum of one crystallite measured after oxygenation
61 in a transmission electron microscope (TEM). The ele-
62 mental composition deduced from the spectrum confirms
63 the atomic ratio 1:1:1 for the elements La, Fe and Si
64 as in the precursor. In addition, we observe an intense
65 peak at 0.525 keV. This peak corresponds to the $K_{\alpha 1}$
66 electronic transition of oxygen, which shows that oxy-
67 gen is present. The inset in Fig. 1 shows the $hk0$ -
68 plane of the 3D electron diffraction patterns obtained
69 from the crystallite. This cut reveals that the tetrago-
70 nal $P4/nmm$ space-group symmetry of the precursor is
71 preserved after oxygenation. Furthermore, the analysis

* Corresponding author. email: pierre.toulemonde@neel.cnrs.fr

72 of the full dataset reveals unambiguously electron den-
 73 sity corresponding to oxygen, occupying the $2b$ Wyckoff
 74 position located at the center of the La_4 tetrahedron (see
 75 Fig. 6 in Supplementary Information (S.I.)). This shows
 76 that the oxygen which was detected by EDX is in fact
 77 present in the crystal structure and is not only a surface
 78 contamination.

79 The refined structural parameters at 300 K from neu-
 80 tron powder diffraction (NPD) are shown in Table I (cor-
 81 responding to the Rietveld fit shown Fig. 2b). The
 82 refinement confirms the presence of oxygen in the La_4
 83 tetrahedron with an occupancy of 0.90(2). Investigat-
 84 ing several samples has shown similar values of the unit
 85 cell parameters, indicating that this occupancy is consis-
 86 tently reached.

87 When comparing to the precursor [8, 9], we observe
 88 a strongly anisotropic expansion of the unit cell, due to
 89 the oxygen inserted in the iso-symmetrical ($P4/nmm$)
 90 structure of LaFeSi . Specifically, the lattice parameters
 91 of $\text{LaFeSiO}_{1-\delta}$ are $a = 4.1085(4)$ Å and $c = 8.132(2)$ Å,
 92 resulting in a change of the c/a ratio from LaFeSi to
 93 $\text{LaFeSiO}_{1-\delta}$, from 1.74 to 1.98.

94 The refined atomic positions, also shown in Table I,
 95 reveal that the z parameter of Si is low, leading to an
 96 anion height $h_{\text{Fe-Si}} = 0.94(1)$ Å. This is considerably lower
 97 than in LaFeAsO where $h_{\text{Fe-As}} = 1.32(1)$ Å [10, 11]. In
 98 $\text{LaFeSiO}_{1-\delta}$, however, the Fe-containing block is chem-
 99 ically different from the arsenides so it may be better
 100 compared to LaFeSiH for which $h_{\text{Fe-Si}} = 1.20(1)$ Å [4].
 101 In any case, the trend is similar to what is seen for
 102 the arsenides where the Fe-As layer is more compressed
 103 in LaFeAsO than the substituted $\text{LaFeAsO}_{1-x}\text{H}_x$ [10].
 104 However, $h_{\text{Fe-Si}}$ in $\text{LaFeSiO}_{1-\delta}$ is far from the geome-
 105 tries recorded for other IBSCs. Considering the corre-
 106 lation between $h_{\text{Fe-Si}}$ and T_c currently proposed in the
 107 literature for iron pnictides or -chalcogenides, this geom-
 108 etry should be detrimental to superconductivity [12].

109 It is also interesting to consider the resulting angle
 110 $\alpha(\text{Si-Fe-Si})$ of the FeSi_4 tetrahedral unit as this is of-
 111 ten used as a measure of the tetrahedral geometry. The
 112 T_c is normally optimised around the regular tetrahedron
 113 value namely $\alpha = 109.47^\circ$ [11, 13–15]. In $\text{LaFeSiO}_{1-\delta}$ the
 114 α angle is found to be $\alpha = 130.9(8)^\circ$, resulting from the
 115 compression of the Fe-Si layer along the c -axis upon in-
 116 sertion of oxygen. This is again far away from the geom-
 117 etry where superconductivity is optimized for arsenides
 118 and it is also away from values found in the fringe case
 119 LaFePO where T_c is below 6 K with an angle of $\alpha = 119.2^\circ$
 120 [16–18].

121 The crystal structure was also measured at low tem-
 122 peratures (2 K and 100 K) using NPD. The unit cell is
 123 contracted at low temperatures and unit cell parameters
 124 reach $a = 4.1019(6)$ Å and $c = 8.090(2)$ Å at 2 K (see
 125 inset of Fig. 2b). In these measurements, no signature
 126 of neither structural distortion nor long-range magnetic
 127 order was detected.

128 Superconducting properties

129 Fig. 3a shows the electrical resistance as a function of
 130 temperature as measured on a small grain of $\text{LaFeSiO}_{1-\delta}$.
 131 The residual resistivity ratio of this grain is around 15
 132 (Fig. 3b), much better than for large cold pressed samples
 133 (~ 2). When measuring these large samples we observe
 134 a drop in the resistance at low temperatures, which is
 135 partial, likely due to insulating grain boundary effects
 136 (see Fig. 9 in S.I.). However, for the small grain, the
 137 drop is complete as we can see in Fig. 3b. This evidences
 138 superconductivity in $\text{LaFeSiO}_{1-\delta}$ with onset $T_c \simeq 10$ K.

139 In Fig. 3c we show the field dependence of T_c up to 7 T
 140 determined for a large cold pressed polycrystalline sam-
 141 ple. By performing a linear fit and using the Werthamer-
 142 Helfand Hohenberg (WHH) formula, we roughly estimate
 143 the upper critical field $H_{c2}(0\text{ K})$ to be ~ 17 T. Since the
 144 T_c is determined from the onset and not from zero re-
 145 sistivity, such value should be considered as an upper
 146 bound for the true thermodynamic H_{c2} .

147 Fig. 3d shows the magnetization difference ΔM be-
 148 tween 2 K and 15 K, i.e. below and just above T_c , as a
 149 function of field. The typical hysteresis loop of a type-II
 150 superconductor is clearly observed. There is also a sig-
 151 nificant ferromagnetic contribution that saturates around
 152 3 T. Nevertheless, the change in magnetization between
 153 2 K and 15 K is dominated by the superconducting phase,
 154 whereas the ferromagnetic contribution, attributed to the
 155 secondary phase $\text{La}(\text{Fe}_{1-x}\text{Si}_x)_{13}$ (see S.I. for a detailed
 156 discussion), changes very little at low T given its very
 157 high Curie temperature $T_{\text{Curie}} > 200$ K [19].

158 Evidence of diamagnetism is further provided by the
 159 negative sign of the zero-field cooled susceptibility, as
 160 measured by the slope of $\Delta M(H)$ (Fig. 3e). The
 161 volumetric susceptibility calculated from the slope is
 162 $\chi_V = -0.15$ which corresponds to 300 times the dia-
 163 magnetic susceptibility of pyrolytic carbon, the strongest
 164 non-superconducting diamagnetic substance known in
 165 the literature [20]. Therefore, the diamagnetic signal ob-
 166 served in these measurements again evidences supercon-
 167 ductivity in $\text{LaFeSiO}_{1-\delta}$.

168 We note that the measured volume susceptibility is a
 169 linear combination of contributions from the supercon-
 170 ducting $\text{LaFeSiO}_{1-\delta}$ phase and the ferromagnetic back-
 171 ground, the two having opposite signs. Therefore, the
 172 apparent susceptibility yields just a lower bound for the
 173 estimate of the superconducting volume fraction, which
 174 is 15%. Such moderate superconducting volume fraction,
 175 as well as the relatively broad transition observed in the
 176 resistivity, may also be linked to chemical inhomogeneity
 177 on the oxygen site arising from the sluggish nature of the
 178 oxygenation process. Hence, despite the refined oxygen
 179 deficit of the sample being $\delta = 0.1$, the actual oxygen
 180 content behind the observed superconductivity at ~ 10 K
 181 may be different and distributed over some small δ range.
 182 However, the slight optimization of T_c in this oxysilicide,
 183 reachable by tuning δ , is out of the scope of the present
 184 study. In any case, the superconducting volume frac-
 185 tion measured in our samples is definitely larger than

186 the amount of secondary phases so that it can safely be
187 attributed to $\text{LaFeSiO}_{1-\delta}$ (for more details see S.I.).

188 Around 30 Oe the magnetization deviates from the lin-
189 ear behaviour observed at low field (Fig. 3e). This gives
190 us an estimate of the lower critical field H_{c1} at 2 K. The
191 magnetization as a function of temperature was also mea-
192 sured, and is shown in Fig. 3f. We observe the Meissner
193 effect as well as a large shielding around 10 K (see zoom
194 in Fig. 8 in S.I.) despite the magnetic background from
195 parasitic phases contributing as a linear slope in the mag-
196 netization.

197 Normal-state properties

198 In the normal state, the resistivity varies as T^α as found
199 in other Fe-based superconductors [21–23]. While enlarg-
200 ing the fitting range tends to decrease α and to degrade
201 the fit quality, a good fit to $T^{1.4}$ is obtained up to 80 K as
202 shown in Fig. 3a. Finding $\alpha \neq 2$ is typical of non Fermi-
203 liquid behavior. Considering the established correlation
204 between the resistivity exponent α and the strength of
205 spin fluctuations [24–26], the value $\alpha \simeq 1.4$ suggests that
206 charge carriers in $\text{LaFeSiO}_{1-\delta}$ are scattered off spin fluc-
207 tuations of similar strength as moderately overdoped Fe-
208 based pnictides, tetragonal $\text{FeSe}_{1-x}\text{S}_x$ [27] or YFe_2Ge_2
209 [28]. As we now explain, the presence of spin fluctua-
210 tions is supported by our ^{29}Si nuclear magnetic resonance
211 (NMR) results.

212 First, we observe that the Knight shift K decreases
213 from room T down to low T (Fig. 4a). As in most Fe-
214 based superconductors of various doping levels, this be-
215 havior reflects the decrease of the static, uniform spin
216 susceptibility $\chi_{\text{spin}}(q=0)$ upon cooling (see for example
217 refs. [25, 26, 29–32]). Visibly, the Fe d electrons produce
218 a transferred hyperfine field at Si sites, just as they do at
219 As/Se sites in iron pnictides/chalcogenides. ^{29}Si NMR
220 thus promises to be a sensitive probe of the electronic
221 properties in this new family of Fe-based superconductors.
222

223 Here, in $\text{LaFeSiO}_{1-\delta}$, we find that the spin-lattice re-
224 laxation rate $1/T_1$ divided by temperature T increases
225 at low T (Fig. 4c), which signifies that the low-energy
226 ($\sim \mu\text{eV}$) spin fluctuations strengthen upon cooling. The
227 observed $\sim 50\%$ enhancement of $1/(T_1T)$ resembles data
228 in the middle of the overdoped regime of 1111 or 122 fam-
229 ilies of iron-based superconductors, for which spin fluc-
230 tuations are relatively weak [25, 26, 29–38]. This ob-
231 servation is consistent with the above described resist-
232 ivity exponent but one should not conclude from this
233 that $\text{LaFeSiO}_{1-\delta}$ has the same doping or the same Fermi
234 surface as moderately overdoped 122 pnictides: for in-
235 stance, a similarly mild enhancement of $1/(T_1T)$ is also
236 found in nonsuperconducting $\text{Fe}_{1.03}\text{Se}$ [39], in tetragonal
237 $\text{FeSe}_{1-x}\text{S}_x$ [31], in LiFeAs [26] and in LiFeP [40]. On
238 the other hand, Fe pnictides with -or close to- spin or-
239 dering [25, 26, 29–38], or even FeSe that does not or-
240 der [39], show much larger enhancement of $1/(T_1T)$ at
241 low T . The relatively weak, albeit tangible, spin fluctua-
242 tions imply that $\text{LaFeSiO}_{1-\delta}$ does not lie in the imme-
243 diate vicinity of a magnetic instability. A difference with

244 $\text{FeSe}_{1-x}\text{S}_x$ and most 1111 or 122 pnictides (a notable
245 exception being $\text{BaFe}_2(\text{As}_{1-x}\text{P}_x)_2$ [24]) is the absence
246 of any discernible activated contribution to $1/(T_1T)$ at
247 high temperatures (typically between 300 K and 100 K),
248 usually attributed to small-momentum fluctuations (so-
249 called intraband transitions [29]). This thus suggests dis-
250 tinctive Fermi surface topology in $\text{LaFeSiO}_{1-\delta}$.

251 The dominant wave vector \mathbf{q} of the fluctuations can-
252 not be determined from the present experiment, so it is
253 not necessarily $(0, \pi)$ in principle. Nevertheless, that the
254 value of the ratio $\alpha_{\text{Korr}} = \hbar \gamma_e^2 / (4 \pi k_B \gamma_n^2) (1/(T_1 T K^2))$
255 (where γ_e and γ_n are the electron and nuclear gyro-
256 magnetic ratio, respectively) largely exceeds 1 and grows
257 upon cooling (Fig. 4f) is an indication that the fluctua-
258 tions are predominantly of antiferromagnetic nature [41],
259 *i.e.* with $\mathbf{q} \neq 0$ (note that in this estimate we have implic-
260 itly assumed that the orbital contribution to K is small
261 compared to the spin contribution and that the hyperfine
262 field at Si sites is relatively isotropic).

263 The NMR data also provide evidence of spatial hetero-
264 geneity, as observed in several Fe-based materials [33–38]:
265 upon cooling below ~ 100 K, the moderate increase of
266 the line width (Fig. 4b) indicates that the distribution
267 of Knight shift values broadens. The concomitant devi-
268 ation from 1 of the stretching exponent β (Fig. 4d and
269 Methods) shows that a distribution of T_1 values develops
270 alongside with the growth of spin fluctuations. The dis-
271 tributed K and T_1 likely stem from spatial variations of
272 the electronic spin polarization around defects [42, 43].

273 Finally, we notice that $1/(T_1T)$ no longer increases be-
274 low 20 K and even drops somewhat below 10 K, that is,
275 below a temperature close to the zero-field T_c (Fig. 4c).
276 This is surprising since the magnetic field of 15 T used
277 in the NMR experiment should be close to the supercon-
278 ducting upper critical field H_{c2} (see above) and thus we
279 would expect to see essentially no sign of superconduc-
280 tivity down to our lowest temperature of 1.7 K. That the
281 stretching exponent β concomitantly reverts its T depen-
282 dence (Fig. 4d) suggests that both the spectral weight
283 and the inhomogeneity of low-energy spin fluctuations
284 are reduced below 10 K. This behavior is unlikely to
285 arise from inhomogeneous superconductivity in the sam-
286 ple or from freezing of spin fluctuations at the NMR
287 timescale [33] as both mechanisms should not lessen the
288 inhomogeneity. More work is however required to under-
289 stand this interesting pseudogap-like behavior that paral-
290 lels earlier observations in LiFeP [40] as well as in Co and
291 F-doped LaFeAsO [37, 38, 44]) and $\text{FeSe}_{1-x}\text{S}_x$ [31, 45].

292 Electronic structure

293 Fig. 5 shows the calculated orbital-resolved density of
294 states (DOS) and the band structure of LaFeSiO . Simi-
295 larly to the reference LaFeAsO compound [46], there is a
296 group of 12 bands between -5.5 eV and 2.5 eV relative
297 to the Fermi energy E_F that come from O- $2p$, Si- $2p$ and
298 Fe- $3d$ states, with the La states contributing at higher
299 energy. The Fe- $3d$ derived bands, in particular, appear
300 between -2.5 eV and 2 eV and dominate the DOS at
301 the Fermi level and thereby the metallic character of the

system. However, the distinct crystal structure of LaFeSiO has a fundamental impact on the low-energy electronic features of this new material. While the Fermi surface preserves the two hole cylinders around the Brillouin zone center (i.e. around the Γ -Z direction), the extra band that crosses the Fermi level and gives rise to the third 3D hole pocket in LaFeAsO is pushed upwards at higher energy. In this way, the hole doping introduced by the As \rightarrow Si substitution is absorbed in a non-rigid-band-shift fashion and results in tiny electron pockets at the zone edge (M-A line). When it comes to superconductivity, however, the band that mainly absorbs this doping remains passive in the standard picture (see e.g. [47]). Moreover, one of the electron pockets around the M-A line loses its Fe- $3d_{x^2-y^2}$ content in favor of a Si- $2p$ character due to the hybridization with the presumably passive band that now crosses the Fermi level at the zone edge and further provides the Fermi-surface sheet with the largest area. This drastically deteriorates the nesting of the Fermi surface, and thereby the tendency towards single-stripe AFM order as we discuss below.

In fact, the fully optimized $P4/nmm$ paramagnetic structure obtained in our DFT calculations agrees remarkably well with the experimental one. Specifically, we find the lattice parameters $a = 4.114 \text{ \AA}$ and $c = 8.144 \text{ \AA}$ with $z_{\text{Si}} = 0.108$ and $z_{\text{La}} = 0.649$, so that the calculated anion height is $h_{\text{Fe-Si}} = 0.88 \text{ \AA}$ (i.e. the difference with the experimental lattice parameters is below 0.7 % while the difference with the experimental $h_{\text{Fe-Si}}$ is 6 %). This is in striking contrast to the pnictides, in particular LaFeAsO, where such a degree of agreement is only obtained in magnetically ordered solutions—thereby revealing a non-trivial magneto-structural interplay [48–50]. This interplay, however, is absent in LaFeSiO.

To further verify this circumstance, we considered the most relevant magnetic orders and we found in fact a much weaker overall tendency towards magnetism. This is the case even at the generalized gradient approximation (GGA) level, which is known to overestimate the magnetism in the Fe-based superconductors [51]. Specifically, while we find a ferromagnetic solution, this is nearly degenerate with the paramagnetic one and has a very low Fe magnetic moment of $\mu_{\text{Fe}} = 0.16 \mu_B$. Furthermore, the single-stripe AFM solution, characteristic of the pnictides, converged to the paramagnetic ($\mu_{\text{Fe}} = 0$) solution. The absence of single-stripe antiferromagnetic solution is indeed totally in tune with the absence of Fermi-surface nesting (Fig. 5c). Still, we find a double-stripe antiferromagnetic solution whose energy difference with respect to the paramagnetic state is just $\Delta E = -5 \text{ meV/Fe}$ with $\mu_{\text{Fe}} = 0.58 \mu_B$ and also a checkerboard one with $\Delta E = -36 \text{ meV/Fe}$ and $\mu_{\text{Fe}} = 1.07 \mu_B$. We note that these magnetization energies are drastically reduced compared to the results obtained assuming LaFeSiO in the reference LaFeAsO structure (i.e. replacing As by Si in LaFeAsO structure) [52]. Consequently, this analysis pinpoints a direct link between the actual unique structure of LaFeSiO and its reduced tendency towards mag-

netism. Overall, the specific fermiology and the modest strength of antiferromagnetic spin fluctuations seen in DFT corroborate the conclusions drawn from the NMR results.

DISCUSSION AND CONCLUSION

In summary, we have reported superconductivity in the new crystallogenic LaFeSiO $_{1-\delta}$. This system displays a drastically reduced anion height $h_{\text{Fe-Si}} = 0.94(1) \text{ \AA}$ and yet superconductivity with onset $T_c = 10 \text{ K}$. In addition, it exhibits relatively weak spin fluctuations, consistent with predictions from first-principles, combined with a non-Fermi-liquid behavior in its normal state. To the best of our knowledge, the conjunction of such structural and superconducting properties is unprecedented in the Fe-based superconducting materials.

For this category of unconventional superconductors, there seems to exist a quasi-universal link between structure and T_c that is further connected to the corresponding fermiology [11, 53]. Thus, the optimal T_c corresponds to having both electron and hole Fermi-surface pockets whose nesting further favors the s_{\pm} -wave mechanism. The hole pockets, however, may disappear as in the strongly electron doped systems or in the intercalated selenides [53]. In this case, superconductivity is believed to require stronger electronic correlations, eventually leading to a d -wave state. LaFeSiO $_{1-\delta}$, however, materializes the opposite situation. Namely, the severe reduction of the anion height is accompanied with a drastic suppression of the initial electron pockets from the Fermi surface. This is obviously detrimental for the s_{\pm} -mechanism, so that the emergence of superconductivity is likely due to stronger correlations, also in tune with its non-Fermi-liquid behavior. However, compared to the chalcogenides, the nature of these correlations is likely different since they originate from a different part of the Fermi surface (i.e. from hole as opposed to electron pockets in the intercalated chalcogenides).

We note that the fermiology of the initial superconducting crystallogenic LaFeSiH and its fluoride LaFeSiF $_{0.7}$ counterpart still matches that of the reference LaFeAsO material [4, 5, 54]. Namely, even if the out-of-plane dispersion becomes significant in LaFeSiH, the Fermi surface of these crystallogenides display the characteristic electron and hole pockets of the Fe-based superconductors. However, this is not the case in LaFeSiO $_{1-\delta}$ as we described above and a similar situation takes place in LaFeSiF $_{0.1}$ [5]. In both these systems the “canonical” electron pockets undergo a dramatic modification while the effective doping with respect to LaFeSiH is mainly absorbed by the otherwise passive band that gives rise to the heavy 3D hole pocket in LaFeAsO [46]. Consequently, despite their apparent difference in doping, these crystallogenides may well belong to a new superconducting dome in the “Lee plot” where the hole pockets become the essential ingredient as we illustrate in Fig. 6. So, beyond further demonstrating the possibility of Fe-based superconductivity in crystallogenides, our findings challenge

417 the current picture of Fe-based superconductivity and are
418 hence expected to motivate further investigations.

419 METHODS

420 Synthesis

421 In order to obtain $\text{LaFeSiO}_{1-\delta}$, the LaFeSi precursor was
422 heated either in air, under an oxygen flow or an emulated
423 air flow (Ar 80 %/ O_2 20 %) for several days. Different
424 conditions were tried in an attempt to control the oxy-
425 gen content. However, this has been unsuccessful and
426 essentially the same stoichiometry was obtained in all in-
427 stances. From a crystallinity point of view, the optimal
428 treatment temperature was found to be 330 °C based on
429 *in-situ* X-ray diffraction (XRD) measurements (Fig. 1
430 in S.I.). The oxygen uptake was also confirmed qualita-
431 tively by thermogravimetric analysis (Fig. 2 in S.I.). The
432 purest $\text{LaFeSiO}_{1-\delta}$ sample batch had a phase purity of
433 96(1) % and was obtained specifically by heating the pre-
434 cursor for 3 days at 330 °C in an emulated air flow consist-
435 ing of 80 % Ar and 20 % O_2 . The ramp which was used
436 for both heating and cooling was 10 °C/min. Secondary
437 phases, already contained in the LaFeSi precursor, per-
438 sist through the oxygenation process. Namely, the ferro-
439 magnetic $\text{La}(\text{Fe},\text{Si})_{13}$ and the paramagnetic LaFe_2Si_2 and
440 correspond to $\sim 2.5(5)\%$ and $\sim 1.5(5)\%$ of the oxygenated
441 sample respectively. The phase purity was estimated by
442 performing a Rietveld fit of X-ray diffraction data (Fig.
443 3 in S.I.).

444 Resistivity

445 The resistivity measurements shown in Fig. 3 (and
446 Fig. 10 in S.I.) correspond to our 96% pure $\text{LaFeSiO}_{1-\delta}$
447 batch. Resistivity was measured on a sample grain
448 of approximately $150\ \mu\text{m} \times 50\ \mu\text{m} \times 50\ \mu\text{m}$. The
449 grain was measured using a 4 circle diffractometer
450 ($\lambda(\text{K}_\alpha(\text{Mo})) = 0.71\ \text{\AA}$) revealing it to be single phase,
451 consisting of a hand full of 1111-type grains. The azimu-
452 tally integrated data can be indexed with the $\text{LaFeSiO}_{1-\delta}$
453 phase determined by NPD, linking the structure and su-
454 perconducting properties.

455 Magnetization

456 The magnetization was measured using the same sample
457 batch as for the resistivity in a Quantum Design MPMS-
458 XL. The sample holder was a thin straw wherein a small
459 pellet of 25.9 mg was fixed using plastic film. The sample
460 was centered without applying an external field. It was
461 then brought to 2 K where upon the field sweep was
462 carried out. The sample was then heated to 300 K in
463 no applied field and cooled to 15 K before once again
464 measuring $M(H)$.

465 Neutron powder diffraction

466 The crystal structure was investigated using neutron
467 powder diffraction on the D1B instrument [55] at the ILL
468 using a wavelength of $\lambda = 1.28\ \text{\AA}$. For this experiment, we
469 used a large sample containing 67(2) % of $\text{LaFeSiO}_{1-\delta}$,
470 $\sim 29(1)\%$ of unreacted LaFeSi and $\sim 4.0(5)\%$ of
471 LaFe_2Si_2 . The crystal structure of $\text{LaFeSiO}_{1-\delta}$ and the
472 proportions of the phases were refined using the Rietveld

473 method in the FULLPROF software [56].

474 X-ray powder diffraction

475 All samples which were produced were investigated by
476 powder XRD, using a D8 Endeavor diffractometer with
477 a $\text{K}_{\alpha 1, \alpha 2}(\text{Cu})$ source. All samples showed similar unit
478 cell parameters.

479 Electron diffraction and energy-dispersive 480 spectroscopy

481 The TEM analysis was performed on a specimen pre-
482 pared by suspending a small amount of powder in
483 ethanol, and depositing a drop of the liquid on a cop-
484 per grid, covered by a holey carbon membrane. The
485 microscope used was a Philips CM300ST (LaB_6 , 300
486 kV) equipped with a F416 TVIPS CMOS camera and
487 a Bruker Silicon Drift Energy Dispersive X-ray Spec-
488 troscopy (EDX) detector. The 3D electron diffraction
489 (ED) study was performed with a tomography sample
490 holder allowing a tilt range of $\pm 50^\circ$, using the method
491 described by S. Kodjikian and H. Klein [57]. ED dataset
492 processing was performed using PETS program, and the
493 crystal structure model was calculated by the charge flip-
494 ping algorithm [58] with the Superflip program [59] in the
495 computing system JANA2006 [60].

496 Nuclear magnetic resonance

497 ^{29}Si measurements were performed in a fixed field of
498 15 T from a superconducting coil, using a home-built
499 heterodyne spectrometer. The field value was calibrated
500 using metallic Cu from the NMR pick-up coil. Knight
501 shift values are given with respect to the bare ^{29}Si reso-
502 nance. Spectra were obtained by adding appropriately-
503 spaced Fourier transforms of the spin-echo signal. The
504 spin-lattice relaxation time T_1 was measured by the
505 saturation-recovery method and the recoveries were fit to
506 the theoretical law for magnetic relaxation of a nuclear
507 spin 1/2: $M(t) = M(\infty)(1 - \exp(-(t/T_1)^\beta))$, modified
508 by an ad-hoc stretching exponent β in order to account
509 for a distribution of T_1 values [61].

510 Electronic structure calculations

511 The main calculations were performed using the
512 all-electron code WIEN2K [62] based on the full-
513 potential augmented plane-wave plus local orbitals
514 method (APW+LO). We considered the Perdew-Burke-
515 Ernzerhof (PBE) form of the generalized gradient ap-
516 proximation (GGA) [63] and used muffin-tin radii of (La)
517 2.30 a.u., (Fe) 2.10 a.u., (Si) 2.10 a.u., and (O) 1.80 a.u.
518 with a plane-wave cutoff $R_{\text{MT}}K_{\text{max}} = 7.0$. Additional
519 calculations were performed with Quantum Espresso [64]
520 using the norm-conserving ONCVSP pseudopotentials
521 from Dojo [65, 66].

522 DATA AVAILABILITY

523 NPD data used for Fig. 2.b and Table I are available at
524 ref.[55]. The other data that support the findings of this
525 study are available from the corresponding author upon
526 reasonable request.

- [1] H. Hosono and K. Kuroki, *Physica C: Superconductivity and its Applications* **514**, 399 (2015).
- [2] C. Lee, K. Kihou, A. Iyo, H. Kito, P. Shirage, and H. Eisaki, *Solid State Communications* **152**, 644 (2012), special Issue on Iron-based Superconductors.
- [3] Y. Mizuguchi, Y. Hara, K. Deguchi, S. Tsuda, T. Yamaguchi, K. Takeda, H. Kotegawa, H. Tou, and Y. Takano, *Superconductor Science and Technology* **23**, 054013 (2010).
- [4] F. Bernardini, G. Garbarino, A. Sulpice, M. Núñez Regueiro, E. Gaudin, B. Chevalier, M.-A. Méasson, A. Cano, and S. Tencé, *Phys. Rev. B* **97**, 100504 (2018).
- [5] J.-B. Vaney, B. Vignolle, A. Demourgues, E. Gaudin, E. Durand, C. Labrugère, F. Bernardini, A. Cano, and S. Tencé, *Nat Commun* **13**, 1462 (2022).
- [6] J. Chen, M. B. Gamza, J. Banda, K. Murphy, J. Tarrant, M. Brando, and F. M. Grosche, *Phys. Rev. Lett.* **125**, 237002 (2020).
- [7] D. Guterding, H. O. Jeschke, I. I. Mazin, J. K. Glasbrenner, E. Bascones, and R. Valentí, *Phys. Rev. Lett.* **118**, 017204 (2017).
- [8] R. Welter, G. Venturini, and B. Malaman, *Journal of Alloys and Compounds* **189**, 49 (1992).
- [9] R. Welter, I. Ijjaali, G. Venturini, and B. Malaman, *Journal of Alloys and Compounds* **265**, 196 (1998).
- [10] H. Hosono and S. Matsuiishi, *Current Opinion in Solid State and Materials Science* **17**, 49 (2013), fe-based Superconductors.
- [11] C.-H. Lee, A. Iyo, H. Eisaki, H. Kito, M. Teresa Fernandez-Diaz, T. Ito, K. Kihou, H. Matsuhata, M. Braden, and K. Yamada, *Journal of the Physical Society of Japan* **77**, 083704 (2008).
- [12] R. S. Kumar, J. J. Hamlin, M. B. Maple, Y. Zhang, C. Chen, J. Baker, A. L. Cornelius, Y. Zhao, Y. Xiao, S. Sinogeikin, and P. Chow, *Applied Physics Letters* **105**, 251902 (2014).
- [13] G. Garbarino, R. Weht, A. Sow, A. Sulpice, P. Toulemonde, M. Álvarez-Murga, P. Strobel, P. Bouvier, M. Mezouar, and M. Núñez Regueiro, *Phys. Rev. B* **84**, 024510 (2011).
- [14] G. Garbarino, R. Weht, A. Sow, C. Lacroix, A. Sulpice, M. Mezouar, X. Zhu, F. Han, H. H. Wen, and M. Núñez-Regueiro, *EPL (Europhysics Letters)* **96**, 57002 (2011).
- [15] T. Saito, S. Onari, and H. Kontani, *Phys. Rev. B* **82**, 144510 (2010).
- [16] J. J. Hamlin, R. E. Baumbach, D. A. Zocco, T. A. Sayles, and M. B. Maple, *Journal of Physics: Condensed Matter* **20**, 365220 (2008).
- [17] Y. Kamihara, H. Hiramatsu, M. Hirano, R. Kawamura, H. Yanagi, T. Kamiya, and H. Hosono, *Journal of the American Chemical Society* **128**, 10012 (2006).
- [18] M. Tegel, I. Schellenberg, R. Pöttgen, and D. Johrendt, *Zeitschrift für Naturforschung B* **63**, 1057 (2008).
- [19] T. Palstra, J. Mydosh, G. Nieuwenhuys, A. van der Kraan, and K. Buschow, *Journal of Magnetism and Magnetic Materials* **36**, 290 (1983).
- [20] A. Kotosonov, *Carbon* **25**, 613 (1987).
- [21] S. Kasahara, T. Shibauchi, K. Hashimoto, K. Ikada, S. Tonegawa, R. Okazaki, H. Shishido, H. Ikeda, H. Takeya, K. Hirata, T. Terashima, and Y. Matsuda, *Phys. Rev. B* **81**, 184519 (2010).
- [22] Y. Zou, Z. Feng, P. W. Logg, J. Chen, G. Lampronti, and F. M. Grosche, *physica status solidi (RRL) - Rapid Research Letters* **8**, 928 (2014).
- [23] J. Yang, R. Zhou, L.-L. Wei, H.-X. Yang, J.-Q. Li, Z.-X. Zhao, and G.-Q. Zheng, *Chinese Physics Letters* **32**, 107401 (2015).
- [24] Y. Nakai, T. Iye, S. Kitagawa, K. Ishida, H. Ikeda, S. Kasahara, H. Shishido, T. Shibauchi, Y. Matsuda, and T. Terashima, *Phys. Rev. Lett.* **105**, 107003 (2010).
- [25] R. Zhou, Z. Li, J. Yang, D. L. Sun, C. T. Lin, and G.-q. Zheng, *Nature Communications* **4**, 2265 (2013).
- [26] Y. M. Dai, H. Miao, L. Y. Xing, X. C. Wang, P. S. Wang, H. Xiao, T. Qian, P. Richard, X. G. Qiu, W. Yu, C. Q. Jin, Z. Wang, P. D. Johnson, C. C. Homes, and H. Ding, *Phys. Rev. X* **5**, 031035 (2015).
- [27] M. Bristow, P. Reiss, A. A. Haghighirad, Z. Zajicek, S. J. Singh, T. Wolf, D. Graf, W. Knafo, A. McCollam, and A. I. Coldea, *Phys. Rev. Research* **2**, 013309 (2020).
- [28] J. Chen, K. Semeniuk, Z. Feng, P. Reiss, P. Brown, Y. Zou, P. W. Logg, G. I. Lampronti, and F. M. Grosche, *Phys. Rev. Lett.* **116**, 127001 (2016).
- [29] F. L. Ning, K. Ahilan, T. Imai, A. S. Sefat, M. A. McGuire, B. C. Sales, D. Mandrus, P. Cheng, B. Shen, and H.-H. Wen, *Phys. Rev. Lett.* **104**, 037001 (2010).
- [30] H. Mukuda, F. Engetsu, K. Yamamoto, K. T. Lai, M. Yashima, Y. Kitaoka, A. Takemori, S. Miyasaka, and S. Tajima, *Phys. Rev. B* **89**, 064511 (2014).
- [31] P. Wiecki, K. Rana, A. E. Böhmer, Y. Lee, S. L. Bud'ko, P. C. Canfield, and Y. Furukawa, *Phys. Rev. B* **98**, 020507 (2018).
- [32] T. Shiroka, N. Barbero, R. Khasanov, N. D. Zhigadlo, H. R. Ott, and J. Mesot, *npj Quantum Materials* **3**, 25 (2018).
- [33] F. Hammerath, U. Gräfe, T. Kühne, H. Kühne, P. L. Kuhns, A. P. Reyes, G. Lang, S. Wurmehl, B. Büchner, P. Carretta, and H.-J. Grafe, *Phys. Rev. B* **88**, 104503 (2013).
- [34] A. P. Dioguardi, J. Crocker, A. C. Shockley, C. H. Lin, K. R. Shirer, D. M. Nisnon, M. M. Lawson, N. apRoberts Warren, P. C. Canfield, S. L. Bud'ko, S. Ran, and N. J. Curro, *Phys. Rev. Lett.* **111**, 207201 (2013).
- [35] H.-J. Grafe, U. Gräfe, A. P. Dioguardi, N. J. Curro, S. Aswartham, S. Wurmehl, and B. Büchner, *Phys. Rev. B* **90**, 094519 (2014).
- [36] A. P. Dioguardi, M. M. Lawson, B. T. Bush, J. Crocker, K. R. Shirer, D. M. Nisnon, T. Kissikov, S. Ran, S. L. Bud'ko, P. C. Canfield, S. Yuan, P. L. Kuhns, A. P. Reyes, H.-J. Grafe, and N. J. Curro, *Phys. Rev. B* **92**, 165116 (2015).
- [37] H.-J. Grafe, P. Lepucki, M. Witschel, A. P. Dioguardi, R. Kappenberger, S. Aswartham, S. Wurmehl, and B. Büchner, *Phys. Rev. B* **101**, 054519 (2020).
- [38] P. Lepucki, R. Havemann, A. P. Dioguardi, F. Scaravaggi, A. U. B. Wolter, R. Kappenberger, S. Aswartham, S. Wurmehl, B. Büchner, and H.-J. Grafe, *Phys. Rev. B* **103**, L180506 (2021).
- [39] T. Imai, K. Ahilan, F. L. Ning, T. M. McQueen, and R. J. Cava, *Phys. Rev. Lett.* **102**, 177005 (2009).
- [40] H. Man, S. Guo, G. Zhi, X. Gong, Q. Wang, C. Ding, Y. Jin, and F. Ning, *EPL (Europhysics Letters)* **105**, 67005 (2014).

- [41] P. Wiecki, B. Roy, D. C. Johnston, S. L. Bud'ko, P. C. Canfield, and Y. Furukawa, *Phys. Rev. Lett.* **115**, 137001 (2015).
- [42] M.-H. Julien, T. Fehér, M. Horvatić, C. Berthier, O. N. Bakharev, P. Ségransan, G. Collin, and J.-F. Marucco, *Phys. Rev. Lett.* **84**, 3422 (2000).
- [43] Y. Xin, I. Stolt, Y. Song, P. Dai, and W. P. Halperin, *Phys. Rev. B* **104**, 144421 (2021).
- [44] S. Kitagawa, Y. Nakai, T. Iye, K. Ishida, Y. Kamihara, M. Hirano, and H. Hosono, *Phys. Rev. B* **81**, 212502 (2010).
- [45] A. Shi, T. Arai, S. Kitagawa, T. Yamanaka, K. Ishida, A. E. Böhmer, C. Meingast, T. Wolf, M. Hirata, and T. Sasaki, *Journal of the Physical Society of Japan* **87**, 013704 (2018).
- [46] D. J. Singh and M.-H. Du, *Phys. Rev. Lett.* **100**, 237003 (2008).
- [47] K. Kuroki, H. Usui, S. Onari, R. Arita, and H. Aoki, *Phys. Rev. B* **79**, 224511 (2009).
- [48] T. Yildirim, *Phys. Rev. Lett.* **101**, 057010 (2008).
- [49] A. Cano, M. Civelli, I. Eremin, and I. Paul, *Phys. Rev. B* **82**, 020408 (2010).
- [50] I. Paul, A. Cano, and K. Sengupta, *Phys. Rev. B* **83**, 115109 (2011).
- [51] I. I. Mazin, M. D. Johannes, L. Boeri, K. Koepernik, and D. J. Singh, *Phys. Rev. B* **78**, 085104 (2008).
- [52] P. V. Arribi, F. Bernardini, L. de' Medici, P. Toulemonde, S. Tencé, and A. Cano, *EPL (Europhysics Letters)* **128**, 47004 (2020).
- [53] R. J. Sun, Y. Quan, S. F. Jin, Q. Z. Huang, H. Wu, L. Zhao, L. Gu, Z. P. Yin, and X. L. Chen, *Phys. Rev. B* **98**, 214508 (2018).
- [54] A. Bhattacharyya, P. Rodière, J.-B. Vaney, P. K. Biswas, A. D. Hillier, A. Bosin, F. Bernardini, S. Tencé, D. T. Adroja, and A. Cano, *Phys. Rev. B* **101**, 224502 (2020).
- [55] M. F. Hansen and V. Nassif, Institut Laue-Langevin (ILL) <http://doi.ill.fr/10.5291/ILL-DATA.5-24-657> (2021).
- [56] J. Rodríguez-Carvajal, *Physica B: Condensed Matter* **192**, 55 (1993).
- [57] S. Kodjikian and H. Klein, *Ultramicroscopy* **200**, 12 (2019).
- [58] L. Palatinus, *Acta Crystallographica Section B* **69**, 1 (2013).
- [59] L. Palatinus and G. Chapuis, *Journal of Applied Crystallography* **40**, 786 (2007).
- [60] V. Petříček, M. Dušek, and L. Palatinus, *Zeitschrift für Kristallographie - Crystalline Materials* **229**, 345 (2014).
- [61] V. F. Mitrović, M.-H. Julien, C. de Vaulx, M. Horvatić, C. Berthier, T. Suzuki, and K. Yamada, *Phys. Rev. B* **78**, 014504 (2008).
- [62] P. Blaha, K. Schwarz, G. Madsen, D. Kvasnicka, J. Luitz, R. Laskowski, F. Tran, and L. D. Marks, (Karlheinz Schwarz, Techn. Universität Wien, Austria). ISBN 3-9501031-1-2 (2018).
- [63] J. P. Perdew, K. Burke, and M. Ernzerhof, *Phys. Rev. Lett.* **77**, 3865 (1996).
- [64] P. Giannozzi, S. Baroni, N. Bonini, M. Calandra, R. Car, C. Cavazzoni, D. Ceresoli, G. L. Chiarotti, M. Cococcioni, I. Dabo, A. D. Corso, S. de Gironcoli, S. Fabris, G. Fratesi, R. Gebauer, U. Gerstmann, C. Gougoussis, A. Kokalj, M. Lazzeri, L. Martin-Samos, N. Marzari, F. Mauri, R. Mazzarello, S. Paolini, A. Pasquarello, L. Paulatto, C. Sbraccia, S. Scandolo, G. Sclauzero, A. P. Seitsonen, A. Smogunov, P. Umari, and R. M. Wentzcovitch, *Journal of Physics: Condensed Matter* **21**, 395502 (2009).
- [65] D. R. Hamann, *Phys. Rev. B* **88**, 085117 (2013).
- [66] M. van Setten, M. Giantomassi, E. Bousquet, M. Verstraete, D. Hamann, X. Gonze, and G.-M. Rignanese, *Comput. Phys. Commun.* **226**, 39 (2018).
- [67] H. Hosono and K. Kuroki, *Physica C: Superconductivity and its Applications* **514**, 399 (2015), superconducting Materials: Conventional, Unconventional and Undetermined.

ACKNOWLEDGEMENTS

We want to thank Jacques Pecaat for his measurement on a 4-circle diffractometer of the sample grain measured in resistivity. We thank Rémy Bruyere, Paul Chometon and Frédéric Gay for assistance in high-temperature XRD, thermogravimetric analysis and resistivity measurements, respectively. We thank the ILL for providing beamtime at the D1B instrument. This work was supported by the ANR-18-CE30-0018-03 Ironman grant and the French state funds ANR-10-LABX-51-01 (Labex LANEF du Programme d'Investissements d'Avenir). F.B. acknowledges support from Cineca ISCR-C project "IsC78-NICKSUP-HP10C91RDL". A.C. acknowledges support from the Visiting Professor/Scientist 2019 program founded by the Regione Autonoma Sardegna.

AUTHOR CONTRIBUTIONS

P.T., S.T. and A.C. designed the research; M.F.H., J.-B.V., C.L., H.M., M.H.J., F.B., E.G, V.N. M.-A.M. and A.C. performed research; M.F.H., J.-B.V., C.L., E.G., A.S. and M.H.J. analysed data, M.F.H, M.H.J., A.C. and P.T wrote the paper.

COMPETING INTERESTS

The authors declare no competing interests.

ADDITIONAL INFORMATION

Correspondence and requests for materials should be addressed to P.T.

$P4/nmm$ (#129, origin 2)					
T = 300 K, $a = 4.1085(4)$ Å, $c = 8.132(2)$ Å.					
Atom	Wyckoff pos.	x	y	z	Occ.
La	$2c$	1/4	1/4	0.6526(9)	1
Fe	$2a$	3/4	1/4	0	1
Si	$2c$	1/4	1/4	0.116(2)	1
O	$2b$	3/4	1/4	1/2	0.90(2)

TABLE I. LaFeSiO_{1- δ} refined crystal structure at 300 K from NPD data (Bragg R-factor = 5.05).

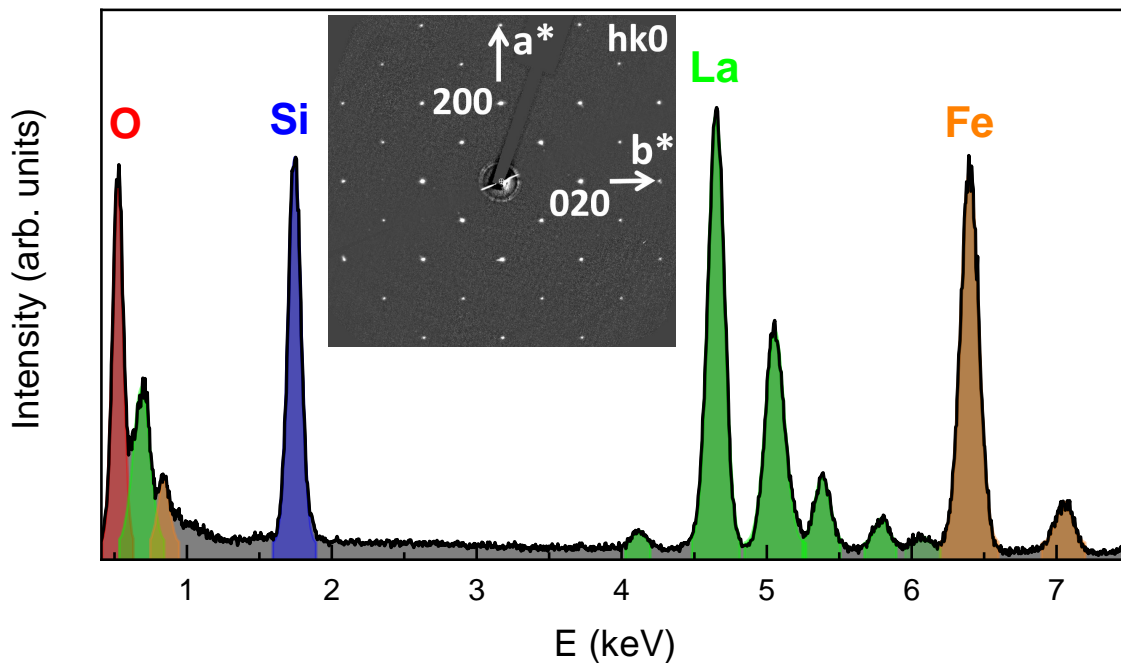


FIG. 1. EDX spectrum recorded on one crystallite showing an oxygen peak at 0.525 keV in the LaFeSi matrix. **Inset:** hk0-cut of the reciprocal space indexed in P4/nmm space group of $\text{LaFeSiO}_{1-\delta}$.

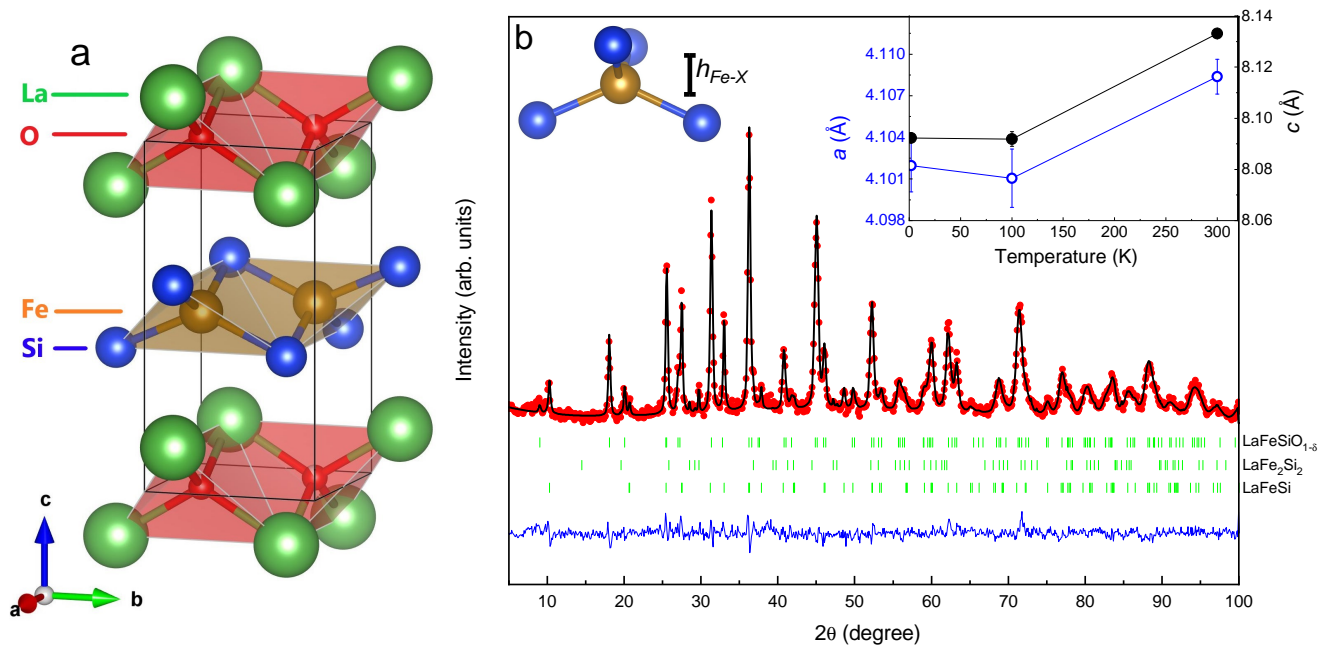


FIG. 2. **a:** The crystal structure as determined by NPD. The structure is shifted by (0,0,0.5) to emphasize the Fe containing layer. **b:** Rietveld refinement of the NPD data collected at 300 K at the D1B instrument of ILL. Three phases are included: $\text{LaFeSiO}_{1-\delta}$, LaFe_2Si_2 and unreacted LaFeSi (from top to bottom). **Inset:** Temperature dependence of a and c lattice parameters.

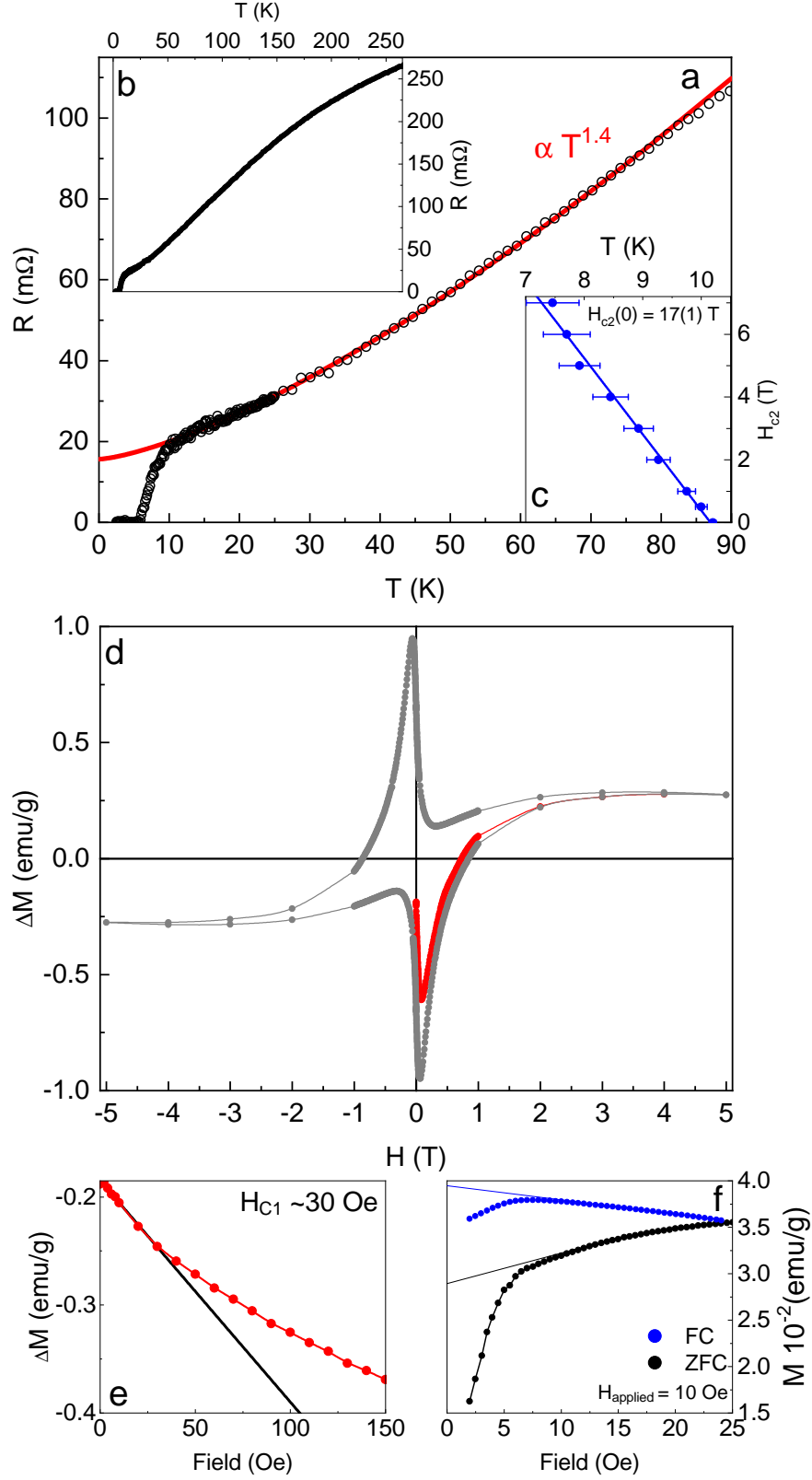


FIG. 3. **a**: Electrical resistance of $\text{LaFeSiO}_{1-\delta}$ as a function of temperature showing superconductivity with onset $T_c = 10$ K and non-Fermi liquid $T^{1.4}$ behavior in the normal state. **b**: Extended plot of the resistance up to room temperature. **c**: Superconducting transition temperature versus applied field. The fit to the WHH formula gives $H_{c2}(0) = 17$ T. **d**: Superconducting hysteresis loop obtained by difference from the magnetization measured at 2 K and 15 K for a cold pressed cylinder of polycrystalline $\text{LaFeSiO}_{1-\delta}$. **e**: A zoom of the initial part of **d**, fitted with a linear expression to obtain the susceptibility. **f**: The field-cooled/zero-field-cooled magnetization curves measured on the same pellet of $\text{LaFeSiO}_{1-\delta}$.

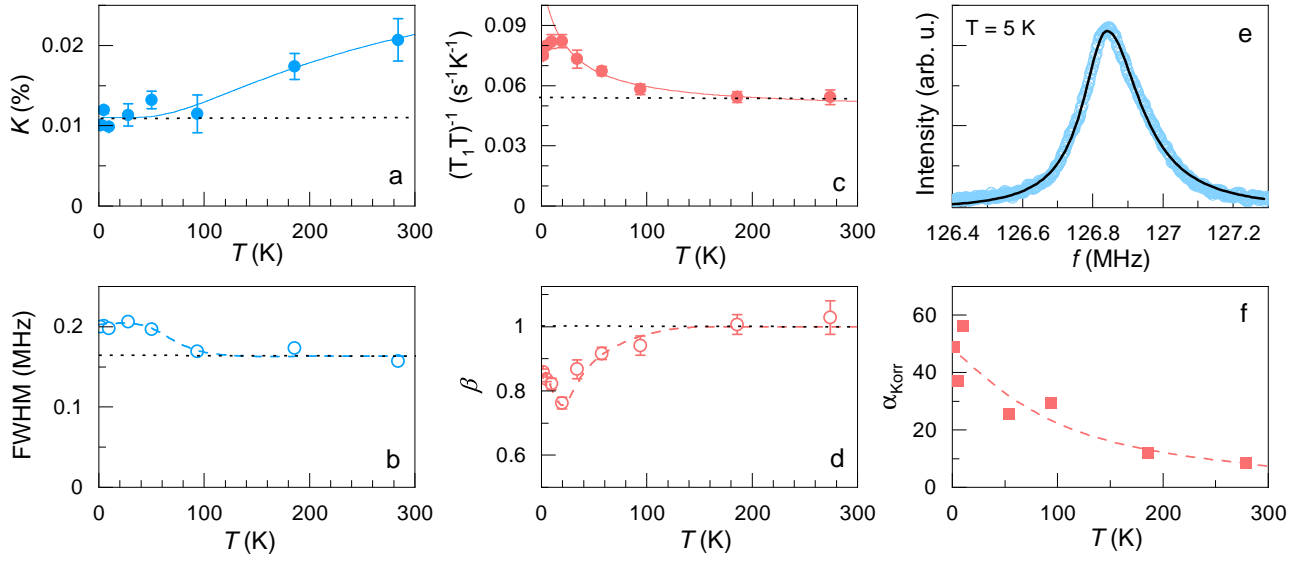


FIG. 4. **a:** Knight shift defined from the peak position of the ^{29}Si resonance shown in panel **e**. The continuous line represents the activated form $K = A + B \exp(-\Delta/k_B T)$, as observed in various Fe-based superconductors, with $\Delta = 250$ K here. **b:** Full width at half maximum of the ^{29}Si resonance shown in panel **e**. The line broadening arises from a distribution of Knight shifts values. The dashed line is a guide to the eye. **c:** Spin-lattice relaxation rate divided by temperature. The continuous line is a fit to the Curie-Weiss form $a+c/(T+\theta)$ with $\theta = 22$ K. **d:** Stretching exponent β used to fit the nuclear recoveries in a T_1 experiment (see Methods). β provides a measure of the width of the distribution of T_1 values. **e:** ^{29}Si NMR line at $T = 5$ K in a field of 15 T. The continuous black line is a fit to an asymmetric Lorentzian form. The slight asymmetry may arise from Knight shift anisotropy as all directions contribute to the spectrum in this powder sample. **f:** Ratio $\alpha_{\text{Korr}} = \hbar \gamma_e^2 / (4\pi k_B \gamma_n^2) (1/(T_1 T K^2))$. $\alpha_{\text{Korr}} \gg 1$ is evidence of predominant antiferromagnetic fluctuations. The dashed lines in panels b, d and f are guides to the eye and the dotted lines in all the panels represent T independent behavior.

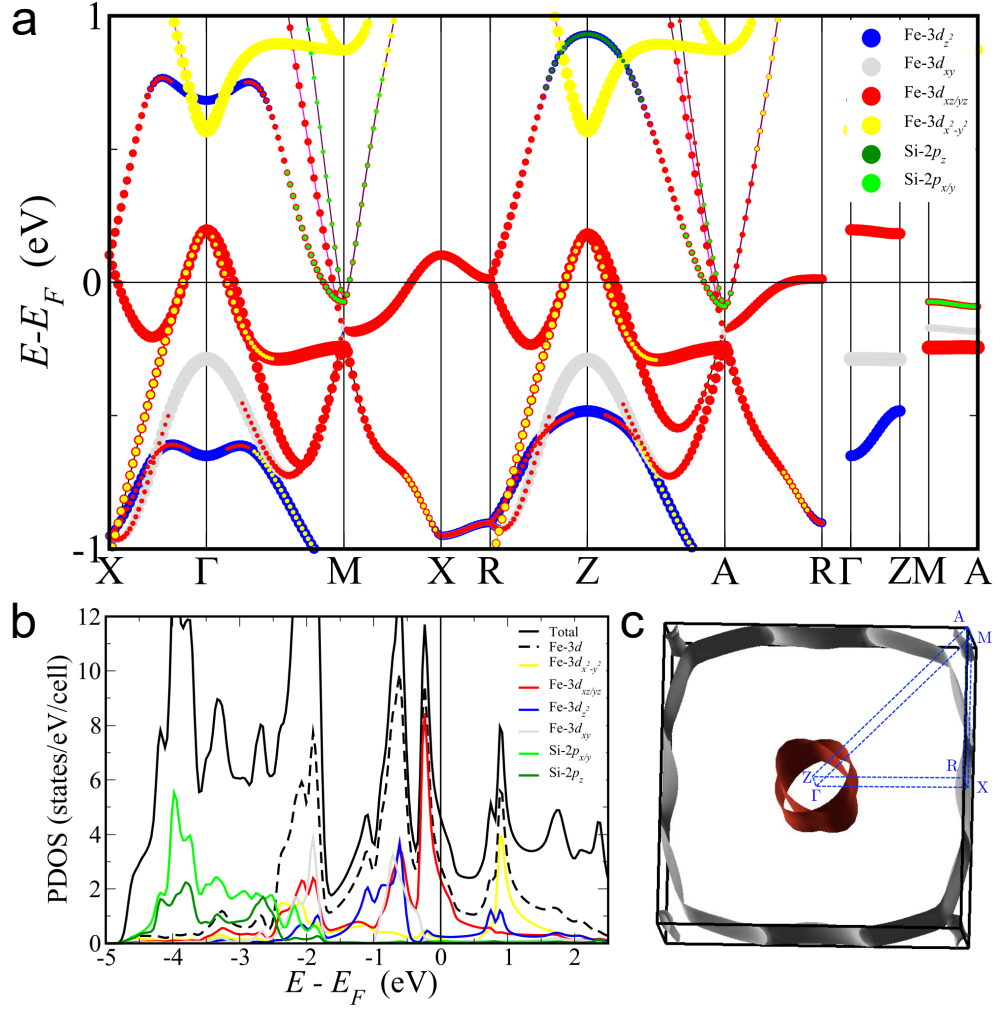


FIG. 5. Calculated electronic structure of LaFeSiO. **a:** Orbital-resolved band structure along the high-symmetry directions of the $P4/nmm$ Brillouin zone. **b:** Orbital-resolved density of states. **c:** Perspective view of Fermi surface computed on the basis of the experimental structure in Table I. The labels indicate the high-symmetry points and lines correspond to the k -path in **a**.

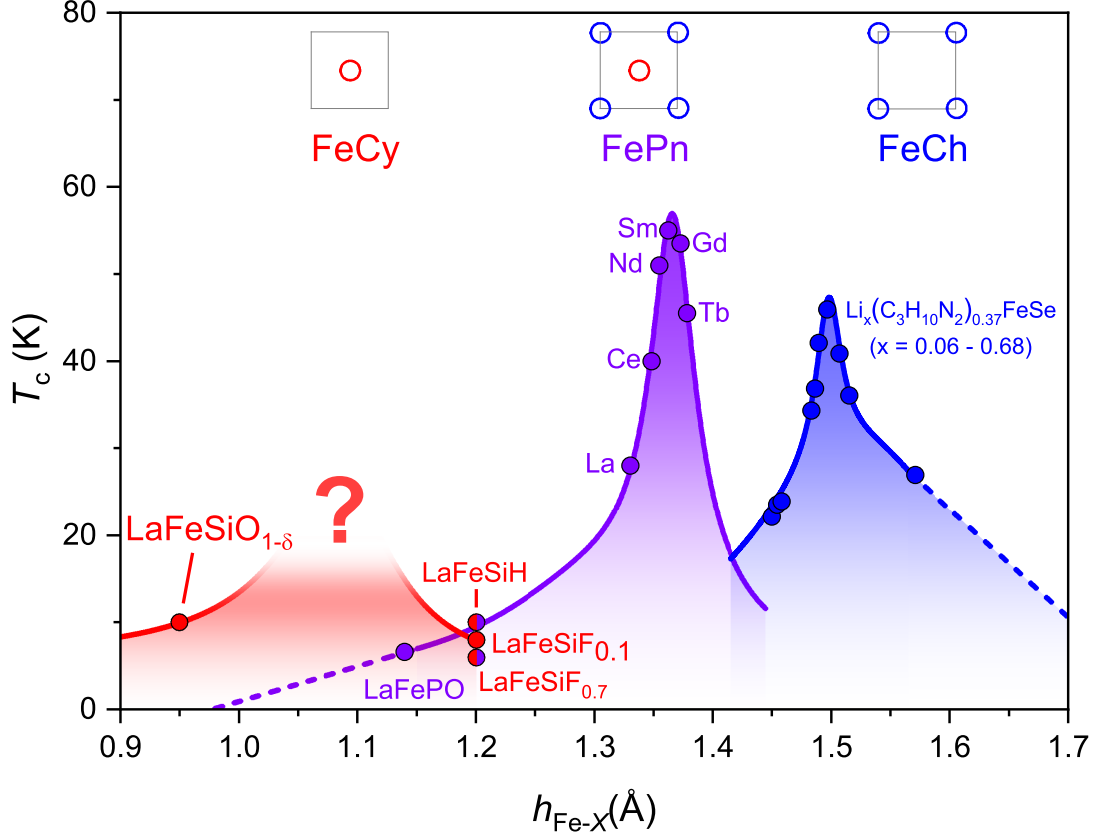


FIG. 6. Superconducting transition temperature T_c as a function of the anion height from the Fe plane $h_{\text{Fe-X}}$ for pnictides (Pn) in purple (labelled with RE for $\text{REFeAsO}_{1-x}(\text{H,F})_x$) [67] (and references therein), heavily electron doped chalcogenides (Ch) in blue [53] and crystallogenides (Cy) in red ($\text{LaFeSiO}_{1-\delta}$ (this work), LaFeSiF_x [5] and LaFeSiH [4]). The sketches illustrate the simplified Fermi surfaces of these materials and LaFeSiH and $\text{LaFeSiF}_{0.7}$ are marked in red/purple to indicate that the fermiology of these crystallogenides bear resemblance to the pnictides. The T_c of the pnictides and chalcogenides peaks at different $h_{\text{Fe-X}}$ values, which can be ascribed to their different fermiology (and hence pairing mechanism). The new superconducting crystallogenide $\text{LaFeSiO}_{1-\delta}$ reported in this work provides yet another fermiology and appears above the tail of the pnictide $T_c(h_{\text{Fe-X}})$ curve. This might reveal another FeSi-based superconducting dome.